Contrib Mineral Petrol (2006) 151: 698–716
DOI 10.1007/s00410-006-0088-1

ORIGINAL PAPER

M.-S. Krienitz · K. M. Haase · K. Mezger
V. Eckardt · M. A. Shaikh-Mashail

Magma genesis and crustal contamination of continental intraplate lavas in northwestern Syria

Received: 13 June 2005 / Accepted: 7 March 2006 / Published online: 21 April 2006

Abstract The Miocene to Quaternary lavas of northwestern Syria range from basanite, alkali basalts, and tholeiites to basaltic andesites, hawaiites, and mugearites. Crustal assimilation and fractional crystallization processes (AFC) modified the composition of the mantle derived magmas. Crustal assimilation is indicated by decreasing Nb/U (52.8–17.9) and increasing Pb/Nd (0.09–0.21) and by variable isotopic compositions of the lavas ($^{87}Sr/^{86}Sr$: 0.7036–0.7048, $^{143}Nd/^{144}Nd$: 0.51294–0.51269, $^{206}Pb/^{204}Pb$: 18.98–18.60) throughout the differentiation. Modeling of the AFC processes indicates that the magmas have assimilated up to 25% of continental upper crust. The stratigraphy of the lavas reveals decreasing degrees and increasing depths of melting with time and the strongly fractionated heavy rare earth elements indicate melt generation in the garnet stability field. Modeling of melt formation based on trace element contents suggests that 8–10% melting of the asthenospheric mantle source produced the tholeiites, whereas basanite and alkali basalts are formed by 2–4% melting of a similar source.

Electronic Supplementary Material Supplementary material is available for this article at http://www.dx.doi.org/10.1007/s00410-006-0088-1 and is accessible for authorized users.

Communicated by J. Hoefs

M.-S. Krienitz · K. M. Haase
Institut für Geowissenschaften der Universität Kiel,
Olshausenstr. 40, 24118 Kiel, Germany

K. Mezger · V. Eckardt
Institut für Mineralogie der Universität Münster,
Corrensstr. 24, 48149 Munster, Germany

M. A. Shaikh-Mashail
Faculty of Civil Engineering, University of Aleppo,
P.O. Box 5427, Aleppo, Syria

Present address: M.-S. Krienitz (✉)
GeoForschungszentrum Potsdam,
Telegrafenberg, 14473 Potsdam, Germany
E-mail: krieni@gfz-potsdam.de
Tel.: +49-331-2881468
Fax: +49-331-2881474

Introduction

Incompatible element and radiogenic isotopic compositions of continental primitive volcanic rocks often differ from lavas erupted in oceanic settings indicating the presence of other magma sources like the asthenosphere or deep mantle plumes. It has been suggested that continental magmas form from sources in the lower part of the subcontinental thermal boundary layer due to adiabatic melting or due to lowering of the solidus by volatiles (e.g., Gallagher and Hawkesworth 1992). Furthermore, magmas from the asthenosphere may react with the subcontinental lithospheric mantle as they rise to the surface (e.g., Ellam and Cox 1991; Wilson and Downes 1991). The subcontinental lithospheric mantle possibly contains regions that have been metasomatized by small degree melts or fluids during previous magmatic episodes and magmas from these portions may have geochemical compositions that significantly differ from asthenospheric melts. Alternatively, the continental intraplate magmas may be modified by the assimilation of crustal wallrocks as well as by crystal fractionation during their ascent. Several and partly energy-dependent thermodynamic models have been developed to model these processes (DePaolo 1981; Aitchenson and Forrest 1994; Spera and Bohrson 2001). Thus, the study of intracontinental basalts may reveal different petrogenetic processes than the study of basalts in oceanic settings.

In this contribution we provide new geochemical and petrological data for a Cenozoic lava suite from northwestern (NW) Syria in order to investigate their petrogenesis within the large scale geological framework. This study shows that fractional crystallization and crustal contamination were important processes during the magma genesis of the volcanic rocks in NW Syria.

Two chemically different groups of magmas were generated from the same mantle source which is probably situated in the asthenosphere. We interpret the volcanic activity in NW Syria to be related to a slab-breakoff process that occurred in this region, where the Arabian plate converges Eurasia, and coincided with the eruption of the lavas.

Geological setting

Large parts of western Arabia are covered by Cenozoic basaltic lava fields related to the formation of the Red Sea, beginning in Miocene times and to the development of the Miocene/Pliocene Dead Sea fault (DSF) system (Bohannon et al. 1989; Nasir and Safarjalani 2000). The evolution of the western Arabian rift system is accompanied by extensive magmatism and several models have been proposed to explain the intraplate magmatic activity in Israel, Jordan, Saudi Arabia, Syria, and southern Turkey. For example, Camp and Roobol (1992) suggested that the volcanism is caused by hot asthenospheric material either channeled northwards from the Afar plume or that another mantle plume exists beneath western Arabia. Alternatively, Stein and Hofmann (1992) suggested that an old plume head was stored beneath the subcontinental lithosphere and that volcanism was triggered during periods of lithospheric extension. In contrast, Keskin (2003) favored a model of slab steepening and breakoff during the collision of the Arabian plate with Eurasia to explain the magma genesis in Eastern Anatolia.

Syria is located at the NW flank of the Arabian peninsula and is covered by several volcanic fields of Miocene to Quaternary age (Fig. 1). Volcanic rocks are concentrated in the western part of Syria in the vicinity of the Dead Sea fault, but other volcanic fields are spread across the whole country (Fig. 1). The present tectonic situation in Syria is the result of the interaction of the Cenozoic plate boundaries with older intraplate features (McBride et al. 1990). Based on Bouguer gravity anomalies Syria can be divided into three major areas: the Rutbah Uplift in the south is separated by the Palmyride Fold Zone from the northern Aleppo Plateau which is covered by relatively undeformed Palaeozoic and Mesozoic sedimentary rocks (Best et al. 1990; Searle 1994; Sharkov et al. 1994). Seismic studies have shown that the depth of the metamorphic basement beneath the plateau is about 6 km and that a crustal thickness of about 40 km is reached in Syria similar to Jordan and Saudi Arabia (El-Isa et al. 1987; Best et al. 1990; Sandvol et al. 1998; Walley 1998; Kumar et al. 2002). Furthermore, geophysical and geochemical data indicate an upper crustal layer of presumably granitic rocks, ranging in depths from about 5 to 20 km and a lower crust, composed of mafic rocks, at depths of about 20–27 km for the NW Arabian plate and southern Syria (Nasir 1992; Nasir and Safarjalani 2000).

The samples for the present study were collected in the NW part of Syria close to the northern termination of the Dead Sea Fault system and its transition into the East Anatolian Fault zone (Fig. 1). The volcanic units in this region are part of a broader volcanic belt occurring on both sides of the Eastern Anatolian Fault zone.

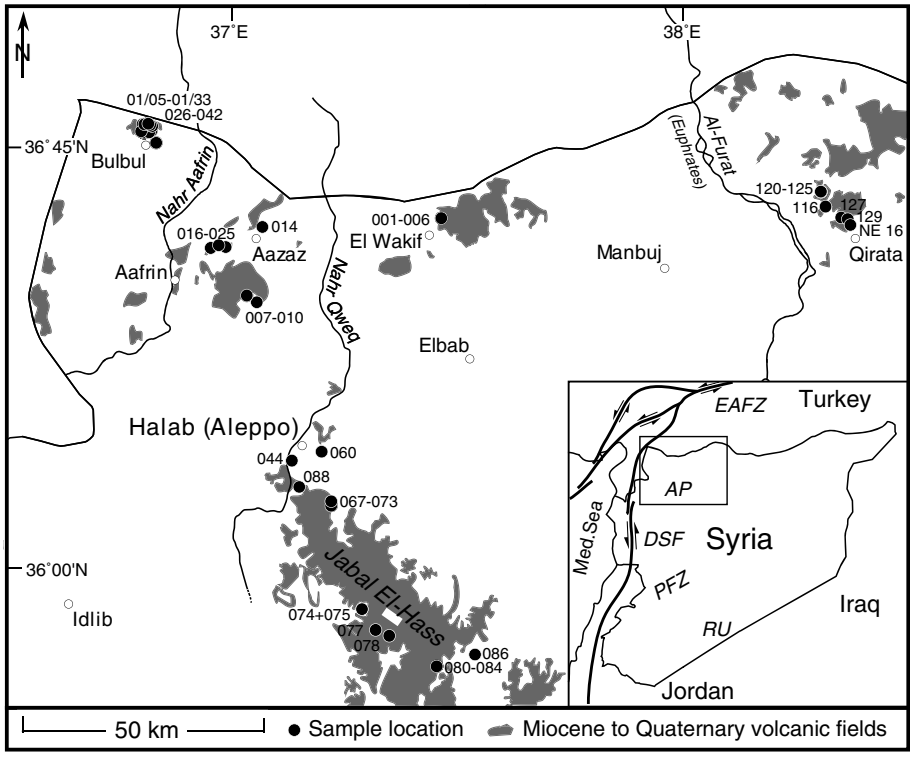

Fig. 1 Location map of northwestern (NW) Syrian volcanic fields with samples locations. *Numbers* beneath sample locations refer to samples names completely listed in Table 2. The *inset* shows the NW part of the Arabian peninsula with active fault zones simplified from Yurtmen et al. (2000). *DSF* Dead Sea Fault, *EAFZ* East Anatolian Fault Zone, *AP* Aleppo Plateau, *PFZ* Palmyride Fold Zone, *RU* Rutbah Uplift. The map is based on geological maps of Ponikarov et al. (1963)

The largest volcanic field located in this part of NW Syria forms the mountain range Jabal El-Hass, with a maximum relief of 300 m and altitude of 640 m (Fig. 1). The volcanic field consists of several lava flows of Miocene age, reaching a total thickness of about 50 m and lying on Paleogene and Neogene sediments (Ponikarov et al. 1963). Single flows vary in thickness from 1 to 10 m and some are separated by thick layers of limestone. Other major volcanic fields, composed of several lava flows, are situated near the villages of Qirata on the eastern side of the Euphrates and around Aazaz and El Wakif (Fig. 1). A lava sequence of about 350 m thickness occurs north of the town Bulbul and was sampled stratigraphically in order to study temporal changes in the petrogenesis (Fig. 1). Petrographically the sequence at Bulbul can be divided into two parts which are separated by a soil horizon suggesting a longer period of volcanic quiescence. Even though Ponikarov et al. (1963) suggested that most of the NW Syrian volcanic units are of upper Pliocene age, Lower Quaternary volcanism occurred around Qirata as indicated by Ar–Ar ages of the upper and lower lavas north of Bulbul yielding Miocene ages between 12 and 10 Ma (Krienitz et al., unpublished data).

Analytical methods

After sawing the freshest parts from each sample, the pieces were washed with deionized water in an ultrasonic bath for 15 min, crushed to coarse sand size with a screw press and washed again. For chemical analysis samples containing fresh glass were handpicked under a binocular microscope. Whole rock samples were reduced to powder in an agate ball mill for major and trace element as well as for radiogenic isotope analysis. Several samples were studied petrographically in thin section and mineral phases were analyzed with a JEOL JXA 8900 electron microprobe operating in wavelength dispersive mode with a beam current of 15 mA (10 mA for glass measurements) and an accelerating voltage of 15 kV. The beam diameter was usually 2 μm and was defocused for feldspar and glass analyses. The measurements were calibrated with mineral standards for the specific elements, and representative mineral and glass analyses are listed in Table 1. Other electron microprobe data of the Syrian samples are given in Electronic Supplementary Material (Table 1).

Major and selected trace (Cr, Ni, Zn, Rb, Sr) elements in Table 1 were analyzed at the Universität Kiel with a Philips PW 1400 XRF using international rock standards for calibration and data quality control. A total of 0.6 g of sample powder was mixed with 3.6 g of flux (lithiumtetraborate) and melted to glass tablets. The accuracy of standard analyses relative to reference values is generally better than 3% for most of the major and trace elements. Only Na_2O and P_2O_5 show higher deviations (8 and 3%, respectively). Replicate measurements of the BHVO-1 standard gave a precision better than 0.30% (SD) for all major elements and generally better than 7.5% (SD) for trace elements (Table 2).

A total of 100 mg of sample material was used for trace and rare earth element (REE) analyses. Measurements were made at the Universität Kiel with an upgraded PlasmaQuad PQ1 ICP-MS following the method of Garbe-Schönberg (1993). Comparison of duplicate digestions of the same sample gave a precision generally better than 1% (SD). The accuracy of the data based on the international rock standard BHVO-1 is better than 7% except for Nb, Ta (< 9%), Sc, Cs and Th (> 9%) and can be estimated from the standard analyses shown in Table 2. A complete list of major, trace, and rare earth element data of the Syrian sample set is given in Electronic Supplementary Material (Table 2).

Most isotope analyses were performed at the Zentrallaboratorium für Geochronologie in Münster using a VG Sector 54 multicollector mass spectrometer operated in dynamic mode for Sr and Nd, and in static mode for Pb isotope ratios (Table 3). A few samples were analyzed in static mode at the GEOMAR Research Center for Marine Geoscience in Kiel for Pb on a Finnigan MAT 262 RPQ2+ and for Sr and Nd on a Finnigan Triton mass spectrometer. For isotopic determinations, about 100 mg of powdered sample material and standard ion exchange techniques were used to separate Sr, Nd and Pb from the matrix. The isotope ratios were corrected for fractionation using $^{86}Sr/^{88}Sr = 0.1194$ and $^{146}Nd/^{144}Nd = 0.7219$. Multiple measurements of the Sr isotope standard NBS 987 in Münster gave 0.710299 (2SD = 0.000026, n = 16) and in Kiel 0.710273 (2SD = 0.000005, n = 8). All Sr isotope analyses were normalized to NBS 987 = 0.710250. The Münster $^{143}Nd/^{144}Nd$ standard runs gave La Jolla: 0.511862 (2SD = 0.000024, n = 14) while in Kiel repeated analysis of the Nd Spex standard yielded 0.511710 (2SD = 0.000005, n = 5) corresponding to a La Jolla value of 0.511828 on the same instrument. The Nd isotope data of the samples were recalculated to a La Jolla value of 0.511850. In Münster, the Pb isotopes were measured in static mode and multiple analyses of the NBS 982 standard were used to correct Pb isotopic ratios for mass fractionation. Standard runs (n = 10) gave $^{206}Pb/^{204}Pb = 36.646$, $^{207}Pb/^{204}Pb = 17.101$, and $^{208}Pb/^{204}Pb = 36.593$ with a precision of ±0.022, ±0.014, and ±0.038 (2SD), respectively. In Kiel standard runs (n = 28) gave $^{206}Pb/^{204}Pb = 16.903$, $^{207}Pb/^{204}Pb = 15.447$, and $^{208}Pb/^{204}Pb = 36.558$ with a precision of ±0.018, ±0.024, and ±0.075 (2SD), respectively. Procedural blanks in both laboratories were generally better than 0.2, 0.1, and 0.04 ng for Sr, Nd, and Pb, respectively.

Results

Classification

According to the total alkali–silica diagram (Le Bas et al. 1986) samples of NW Syria can be classified as

Table 1 Representative microprobe analyses of glasses and minerals of Syrian lavas

Phase	PLAG	CPX	OL	MGT	PLAG	PLAG	CPX	CPX	PLAG	PLAG	PLAG	CPX	OL	OL	GL		GL	
Sample	SY-127	SY-127	SY-127	SY-127	SY-069	SY-080	SY-080	SY-088	SY-033	SY-028	SY-028	SY-039	SY-028	SY-039	SY-023gl		SY-024gl	
Host rock	AB matrix	AB matrix	AB core	AB matrix	T matrix	BA matrix	BA matrix	T matrix	H matrix	M core	M rim	H matrix	M matrix	H matrix	BA		BA	
															(Mean, $n=13$)	SD	Mean, $n=13$)	SD
SiO_2[a]	51.59	46.03	40.15	0.07	51.58	52.56	53.30	51.72	52.04	52.95	53.60	51.09	35.69	34.31	55.26	0.27	55.28	0.39
TiO_2	–	3.85	0.05	28.46	0.11	–	0.60	0.99	–	–	–	1.38	0.14	–	2.05	0.04	2.04	0.06
Al_2O_3	30.94	6.81	0.04	2.83	30.33	30.03	1.08	1.63	29.98	29.76	28.97	2.23	0.03	0.05	14.67	0.09	14.65	0.21
FeO^T	0.51	8.20	14.47	64.65	0.59	0.51	11.57	10.60	0.64	0.48	0.59	9.97	33.85	45.82	10.30	0.15	10.31	0.13
MnO	–	0.13	0.16	0.61	0.04	–	0.33	0.25	–	–	–	0.29	0.52	0.83	0.12	0.04	0.12	0.05
MgO	–	11.36	44.98	2.08	0.12	–	17.95	13.96	–	–	–	14.08	28.47	18.95	4.72	0.08	4.74	0.11
CaO	13.15	21.99	0.23	0.06	12.84	12.86	14.47	20.00	12.80	12.56	11.53	20.01	0.32	0.47	8.07	0.08	8.02	0.08
Na_2O	3.70	0.56	–	0.04	3.90	3.95	0.20	0.52	4.10	4.15	4.60	0.33	0.01	–	3.26	0.17	3.40	0.09
K_2O	0.24	0.03	–	0.01	0.19	0.12	0.01	–	0.26	0.22	0.25	–	–	–	0.97	0.03	0.97	0.04
P_2O_5	–		–		–	–	–	–	–	–	–	–	–	–	0.32	0.04	0.31	0.02
Cr_2O_3	–	0.04	0.02	0.01	0.04	–	0.15	0.04	–	–	–	0.14	0.06	0.02	0.05	0.04	0.05	0.04
NiO	–		–		–	–	–	–	–	–	–	–	–	0.03	–	–	–	–
Total	100.13	99.00	100.10	98.83	99.74	100.03	99.66	99.71	99.82	100.11	99.54	99.52	99.09	100.48	99.91	0.37	100.00	0.44
Albite	33				35	35			36	37	41							
Anorthite	65				64	64			62	62	57							
Orthoclase	1				1	1			1	1	1							
Enstatite		36					52	41				41						
Ferrosilite		14					19	17				16						
Wollastonite		50					30	42				42						
Forsterite			85										60	42				
Ulvöspinel				83														

PLAG plagioclase, *CPX* clinopyroxene, *OL* olivine, *MGT* magnetite, *GL* glass, *AB* alkali basalt, *BA* basaltic andesite, *H* hawaiite, *M* mugearite, *T* tholeiite
[a]Major elements in wt%

Table 2 Representative major (XRF) and trace element (XRF, ICP-MS) analyses of the Syrian samples

Sample	SY 01/10	SY 01/12	SY 01/23	SY-004	SY-010	SY-014	SY-027	SY-028	SY-031	SY-067	SY-127	BHVO-1 (XRF)	BHVO-1 (ICPMS)
Latitude (°N)	36°47′13″	36°46′57″	36°47′08″	36°37′29″	36°29′03″	36°36′34″	36°45′30″	36°46′44″	36°46′44″	36°06′56″	36°37′35″		
Longitude (°E)	36°49′27″	36°49′48″	36°49′07″	37°28′09″	37°02′18″	37°04′26″	36°50′12″	36°48′53″	36°48′53″	37°13′40″	37°19′46″		
Elevation (m)	989	897	875	530	488	603	680	1125	1058	538	392		
Rock type	H	M	T	T	AB	BA	BAS	M	H	BA	AB	Standard	Standard
SiO_2[a]	49.43	50.80	49.96	49.92	45.69	52.12	44.23	51.08	49.78	50.16	44.29	50.00	–
TiO_2	2.23	2.02	1.90	1.39	1.95	1.74	2.52	1.93	2.22	1.66	2.68	2.79	–
Al_2O_3	14.73	16.16	15.79	14.39	14.81	14.84	14.23	16.02	15.01	13.87	12.59	13.86	–
$Fe_2O_3^T$	12.03	11.37	11.63	11.64	11.53	10.73	13.45	11.72	12.47	11.55	13.21	12.26	–
MnO	0.14	0.14	0.16	0.14	0.15	0.13	0.18	0.14	0.17	0.15	0.18	0.17	–
MgO	5.82	4.11	5.22	7.74	5.22	5.17	9.34	4.85	5.48	6.31	9.72	7.23	–
CaO	8.47	8.12	8.42	9.28	11.48	9.61	9.35	8.14	8.82	9.99	10.61	11.54	–
Na_2O	3.61	3.66	3.77	3.21	3.50	3.31	3.48	3.82	3.67	3.27	2.68	2.43	–
K_2O	1.33	1.31	1.00	0.54	0.96	0.83	1.55	1.35	1.33	0.45	1.38	0.53	–
P_2O_5	0.49	0.35	0.29	0.17	0.47	0.22	1.10	0.49	0.61	0.20	0.52	0.28	–
LOI	0.75	0.70	0.51	1.19	2.39	2.15	1.17	1.20	1.00	2.47	1.95	–	–
Total	99.03	98.74	98.65	99.61	98.15	100.85	100.60	100.74	100.56	100.08	99.81	101.09	–
Mg no[b]	0.50	0.43	0.48	0.61	0.51	0.53	0.62	0.49	0.51	0.56	0.63	–	–
Li	8.06	9.34	9.56	8.84	10.7	2.35	8.20	6.72	7.58	10.1	6.09	–	4.45
Sc	19.8	20.9	20.6	19.4	20.6	12.3	17.7	20.4	16.5	15.0	21.2	–	28.7
V	221	223	220	–	–	109	185	205	–	–	239	–	332
Cr	266	162	215	283	211	176	242	171	258	279	283	291	293
Co	40.0	35.6	38.2	48.0	41.3	26.3	48.7	36.2	42.5	44.5	56.4	–	43.9
Ni	114	40.9	63.8	209	82.2	65.3	179	70.5	91	233	211	119	115
Cu	35.4	26.2	32.9	58.0	37.5	29.2	67.6	25.9	32.7	74.2	57.8	–	132
Zn	126	111	113	98.2	98.4	76.0	105	109	121	112	108	104	101
Ga	35.2	34.1	30.5	–	–	–	–	24.2	22.5	20.4	21.9	–	22.2
Rb	28.6	26.5	14.1	11.0	16.6	19.1	19.9	30.9	27.8	6.74	19.3	11	9.56
Y	23.7	25.4	23.3	16.8	20.3	19.6	21.8	24.5	26.6	20.5	19.6	–	24.7
Cs	0.360	0.412	0.187	0.265	0.191	0.654	0.328	0.470	0.293	0.155	0.200	–	0.094
Sr	612	505	423	279	589	301	980	589	670	293	691	401	390
Ba	355	298	237	365	712	568	458	371	360	1533	308	–	133
Zr	164	161	137	86.1	127	114	230	158	164	86.7	182	–	168
Hf	4.36	4.30	3.81	2.57	3.77	3.68	5.93	3.48	4.04	2.43	4.22	–	4.50
Nb	29.6	22.6	16.2	9.01	22.6	12.6	59.7	23.8	31.7	9.97	41.7	–	17.7
Ta	1.59	1.21	0.910	0.625	1.36	0.956	3.51	1.18	1.76	0.608	2.71	–	1.13
Pb	5.02	5.07	3.93	1.54	2.95	3.56	4.43	5.10	4.88	1.69	2.39	–	2.10
Th	4.48	4.03	2.97	1.44	3.29	2.90	9.60	4.50	4.43	1.04	2.96	–	1.22
U	1.06	1.02	0.646	0.442	0.553	0.748	2.69	1.15	1.09	0.331	0.789	–	0.425
La	30.8	24.9	16.8	8.68	26.9	14.4	69.6	31.0	33.4	8.13	25.6	–	15.2
Ce	60.4	48.3	35.5	19.3	55.6	30.4	122	62.6	67.5	18.1	54.1	–	37.9
Pr	7.65	6.37	4.57	2.54	6.63	4.02	12.8	7.16	8.23	2.39	6.35	–	5.34
Nd	31.3	26.4	19.6	11.3	26.9	17.2	46.7	28.0	33.2	10.9	25.9	–	24.4
Sm	6.81	6.06	4.90	3.13	5.86	4.45	8.65	5.88	7.12	3.32	5.84	–	6.16
Eu	2.13	1.91	1.62	1.12	1.87	1.46	2.66	1.95	2.16	1.26	2.01	–	2.03
Gd	6.48	6.12	5.14	3.62	5.80	4.79	8.11	5.71	6.73	3.92	5.65	–	6.11
Tb	0.953	0.943	0.817	0.588	0.832	0.789	1.05	0.807	0.937	0.642	0.799	–	0.933
Dy	5.20	5.37	4.76	3.56	4.66	4.60	5.42	4.41	5.16	3.89	4.20	–	5.30
Ho	0.953	1.03	0.923	0.679	0.861	0.871	0.944	0.815	0.939	0.730	0.737	–	0.979

Table 2 (Contd.)

Sample	SY 01/10	SY 01/12	SY 01/23	SY-004	SY-010	SY-014	SY-027	SY-028	SY-031	SY-067	SY-127	BHVO-1 (XRF)		BHVO-1 (ICPMS)
Latitude (°N)	36°47′13″	36°46′57″	36°47′08″	36°37′29″	36°29′03″	36°36′34″	36°45′30″	36°46′44″	36°46′44″	36°06′56″	36°37′35″			
Longitude (°E)	36°49′27″	36°49′48″	36°49′07″	37°28′09″	37°02′18″	37°04′26″	36°50′12″	36°48′53″	36°48′53″	37°13′40″	37°19′46″			
Elevation (m)	989	897	875	530	488	603	680	1125	1058	538	392			
Rock type	H	M	T	T	AB	BA	BAS	M	H	BA	AB	Standard		Standard
Er	2.42	2.68	2.41	1.75	2.20	2.28	2.31	2.16	2.35	1.85	1.77	–		2.47
Tm	0.318	0.364	0.336	0.235	0.300	0.309	0.297	0.320	0.312	0.244	0.232	–		0.323
Yb	2.00	2.30	2.09	1.52	1.88	1.92	1.79	1.93	1.91	1.48	1.40	–		1.98
Lu	0.276	0.330	0.303	0.217	0.269	0.274	0.254	0.264	0.265	0.203	0.185	–		0.273

Averages of analyses of the standard BHVO-1 (XRF: $n = 7$; ICP-MS: $n = 9$) are also given
BAS basanite, *AB* alkali basalt, *BA* basaltic andesite, *BAS* basanite, *H* hawaiite, *M* mugearite, *T* tholeiite
[a]Major elements in wt%, trace elements in ppm
[b]Mg no = $Mg/(Mg + Fe^{2+})$, assuming $FeO = 0.85Fe^{T}$

basalts and one basanite as well as basaltic andesites, hawaiites, and mugearites (Fig. 2). Basaltic samples include both nepheline- and hypersthene-normative compositions and can thus be further classified as alkali basalts and tholeiites.

Petrography

Alkali basalts and basanite

All analyzed Si-undersaturated samples have porphyritic textures and phenocrysts make up to 20 vol.%. The groundmass consists of plagioclase (An_{65-44}), clinopyroxene (Wo_{50-47}-En_{41-36}), olivine (Fo_{60-56}), and Ti-magnetite (Table 1). Some samples show calcite vesicle fillings. Olivine is the most common phenocryst phase and is more abundant than clinopyroxene. Most olivine phenocrysts are subhedral to skeletal and all show iddingsite rims or are completely altered. The olivine composition indicate that the alkali basalts represent melts that are already fractionated and that the most primitive rocks of the investigated samples are probably not primary melts. One sample contains a clinopyroxene cumulate with resorbed and mostly broken crystals. Sample SY-127 contains an agglomerate of spherical olivine crystals (Fo_{85-82}) that are interpreted as xenocrysts (Table 1).

Tholeiites and basaltic andesites

Plagioclase (An_{64-12}), clinopyroxene (Wo_{44-30}-En_{52-41}), Ti-magnetite, and rarely olivine (Fo_{75-73}) occur in the groundmass of tholeiites and basaltic andesites (Table 1). Some contain vesicles filled with calcite. The samples SY-023 and SY-024 are glass-breccias containing fresh glass fragments of basaltic andesitic compositions in a calcareous matrix (Table 1). The samples contain different amounts of olivine (Fo_{82-55}), clinopyroxene (tholeiite: Wo_{45-44}-En_{44-46}), and plagioclase (An_{65-29}) phenocrysts (Table 1). In the tholeiites olivines are the most abundant phenocryst phase (< 10 vol.%). In contrast, basaltic andesites contain only up to 5 vol.% phenocrysts and partly resorbed xenocrysts. Plagioclase phenocrysts (5–10 vol.%) dominate in most cases over olivine. Cumulate aggregates of plagioclase and clinopyroxene and minor amounts of olivine are observed in both the tholeiites and the basaltic andesites.

Hawaiites and mugearites

The groundmass of hawaiites and mugearites is composed of plagioclase laths (An_{62-20}), clinopyroxene (Wo_{45-42}-En_{41-38}), Ti-magnetite, and rare olivine (Fo_{60-42}) (Table 1). Resorbed quartz crystals occur as xenocrysts in several samples (e.g., SY-028). Plagioclase phenocrysts (An_{65-48}) form euhedral to subhedral, lath-shaped crystals and make up to 5–20 vol.% and in most samples

Table 3 Sr, Nd and Pb isotopic compositions of selected samples of the Syrian lavas

Sample	$^{87}Sr/^{86}Sr$ (2σ)	$^{143}Nd/^{144}Nd$ (2σ)	$^{206}Pb/^{204}Pb$	$^{207}Pb/^{204}Pb$	$^{208}Pb/^{204}Pb$
SY 01/09	0.704749 (10)	0.512732 (13)			
SY 01/10	0.704592 (11)	0.512749 (12)			
SY 01/12	0.704882 (14)	0.512699 (14)	18.844	15.686	38.974
SY 01/23	0.704878 (18)	0.512706 (07)			
SY 01/25	0.704526 (22)	0.512752 (05)			
SY 01/28	0.704378 (12)	0.512819 (11)			
SY 01/29	0.704855 (13)	0.512732 (14)	18.952	15.704	39.050
SY 01/32	0.704745 (22)	0.512749 (06)			
SY-010	0.704066 (03)	0.512803 (03)	18.975	15.671	39.057
SY-028	0.704843 (16)	0.512703 (15)			
SY-033	0.704570 (17)	0.512721 (11)			
SY-037	0.704310 (11)	0.512895 (17)	18.935	15.691	39.036
SY-038	0.704600 (19)	0.512799 (11)			
SY-067	0.704215 (10)	0.512899 (12)	18.605	15.656	38.547
SY-074	0.704747 (10)	0.512781 (13)	18.987	15.648	38.818
SY-082	0.704276 (03)	0.512786 (03)	18.666	15.675	38.516
SY-088	0.703947 (13)	0.512899 (10)	18.828	15.657	38.724
SY-123	0.704223 (12)	0.512795 (11)	18.784	15.652	38.875
SY-127	0.703697 (10)	0.512909 (15)	18.843	15.622	38.767
SY-129	0.703882 (11)	0.512940 (11)	18.778	15.610	38.667

are more abundant than olivine (Fo_{83-50}) and clinopyroxene (Wo_{46-41}-En_{48-38}) which together make up only 5–10 vol.%. The subhedral to skeletal olivine phenocrysts always show iddingsite rims or are totally altered. Some calcite vesicle fillings are observed and several samples contain cumulate aggregates of clinopyroxene and plagioclase crystals.

Chemical alteration

Weathering may cause chemical alteration of rocks affecting especially the mobile elements (e.g., Cs, Rb, K, and U) and leading to a loss of these elements and to elevate H_2O (i.e., loss on ignition = LOI) contents. Concentrations of mobile elements in the whole sample suite do not correlate with MgO contents and LOI. Some alkali basalts, tholeiites, and basaltic andesites have LOI values >2 wt% (up to 3.55 wt%, Table 2) and show the lowest K_2O and U concentrations. If alteration processes have affected these samples, they should have high Nb/U ratios with respect to fresh lavas (Fig. 5a). However, samples with low U concentrations are indistinguishable from the rest of the sample suite in terms of Nb/U ratios. Thus, chemical alteration plays no important role and generally did not affect the mobile elements and has no significant influence on variations of other major and trace elements.

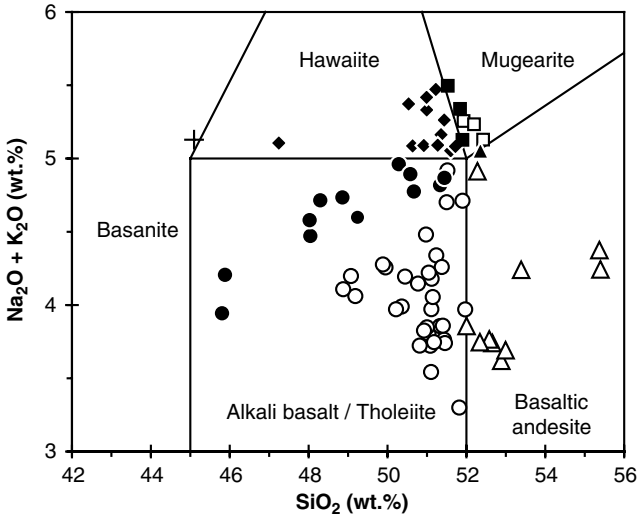

Fig. 2 Total alkali–silica diagram of Le Bas et al. (1986) with rock type discrimination after Le Maitre et al. (1989) for the classification of NW Syrian samples. *Filled symbols* refer to high-P group and *open symbols* to low-P group samples (see text for details)

Geochemistry

Based on their P_2O_5 contents (Fig. 3a) the whole sample suite can be divided into two groups: (1) a high-P group including most of the alkali basalts and mugearites, hawaiites and some of the tholeiites and (2) a low-P group including most of the tholeiites and basaltic andesites and some of the alkali basalts and mugearites (Fig. 2). Although the basanitic sample lies off the trends shown in Fig. 3a, the major and trace element compositions of the basanite are similar to samples of the high-P group (Figs. 3, 4) and thus the basanite will be included in the high-P group. On average samples of the high-P group also have higher TiO_2 and K_2O for a given MgO compared to the low-P group. Even though there is some overlap in terms of SiO_2 contents between the two groups most of the high-P group lavas have lower SiO_2 for a given MgO (Fig. 3). The MgO concentrations of the whole sample suite range from about 10 to 4 wt%. Both lava series generally exhibit negative correlations of Al_2O_3 and Na_2O versus MgO whereas FeO^T, K_2O, and P_2O_5 concentrations are relatively constant over the whole MgO range (Fig. 3). For the low-P group samples

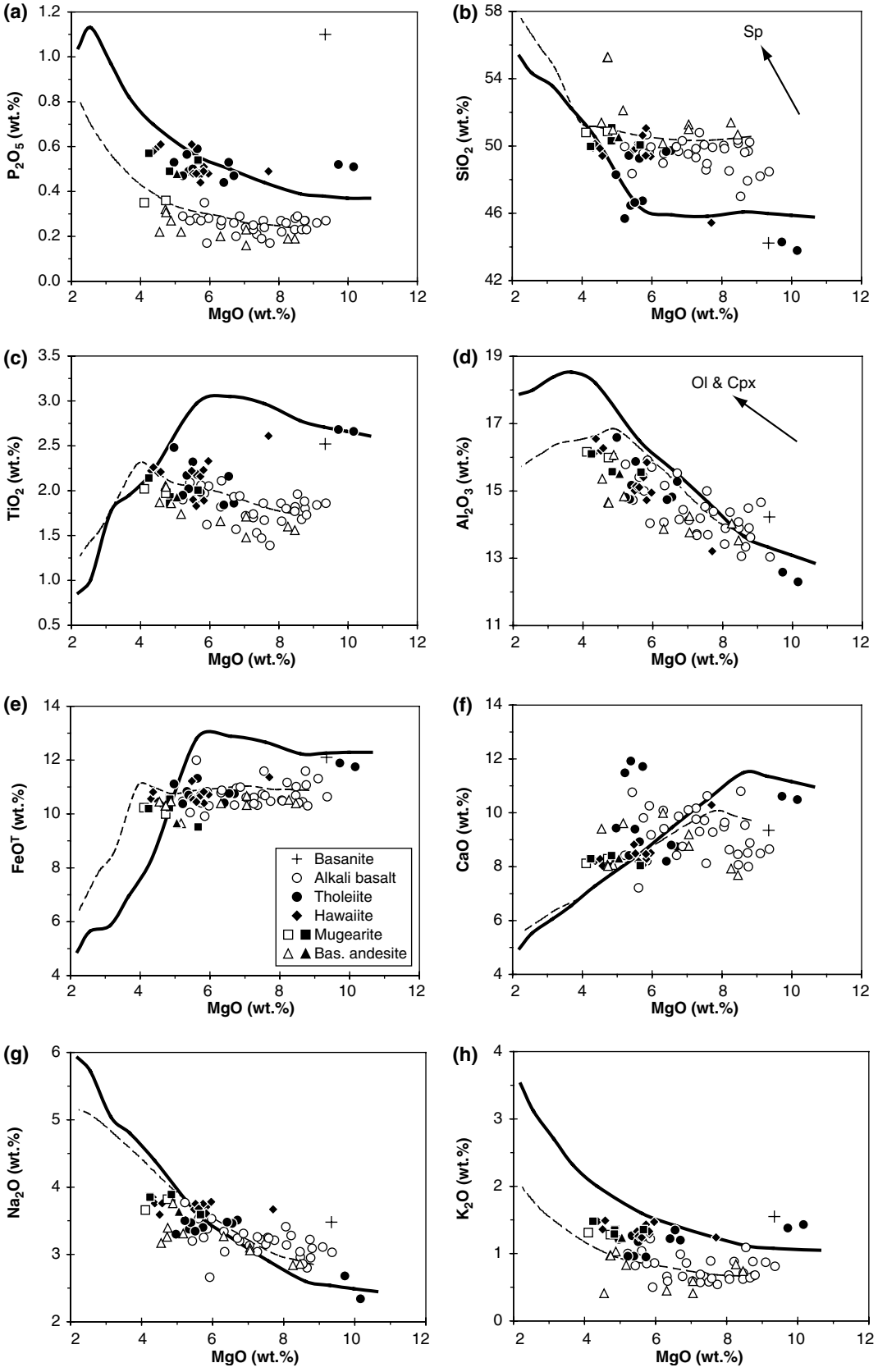

Fig. 3 Selected major element variation diagrams versus MgO. *Arrows* indicate individual fractionation trends of olivine (*ol*), clinopyroxene (*cpx*), and spinel (*sp*). Also shown are results for fractional crystallization modeling using the software program MELTS of Ghiorso and Sack (1995) with input parameters listed in Table 4. Fractional crystallization trends for high-P group samples are given by *continuous lines* and for low-P group samples by *dashed lines*

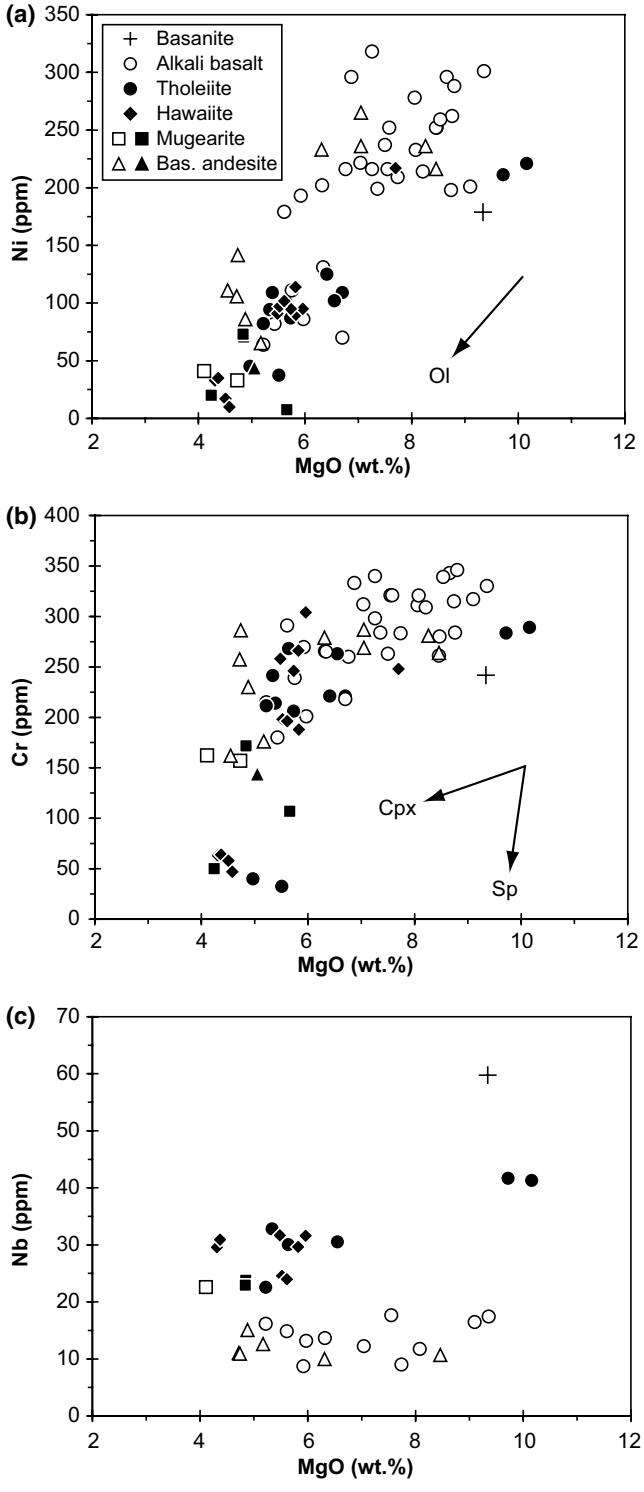

Fig. 4 Plots of the trace elements Ni, Cr, and Nb versus MgO. *Arrows* indicate individual fractionation trends of olivine (*ol*), clinopyroxene (*cpx*), and spinel (*sp*)

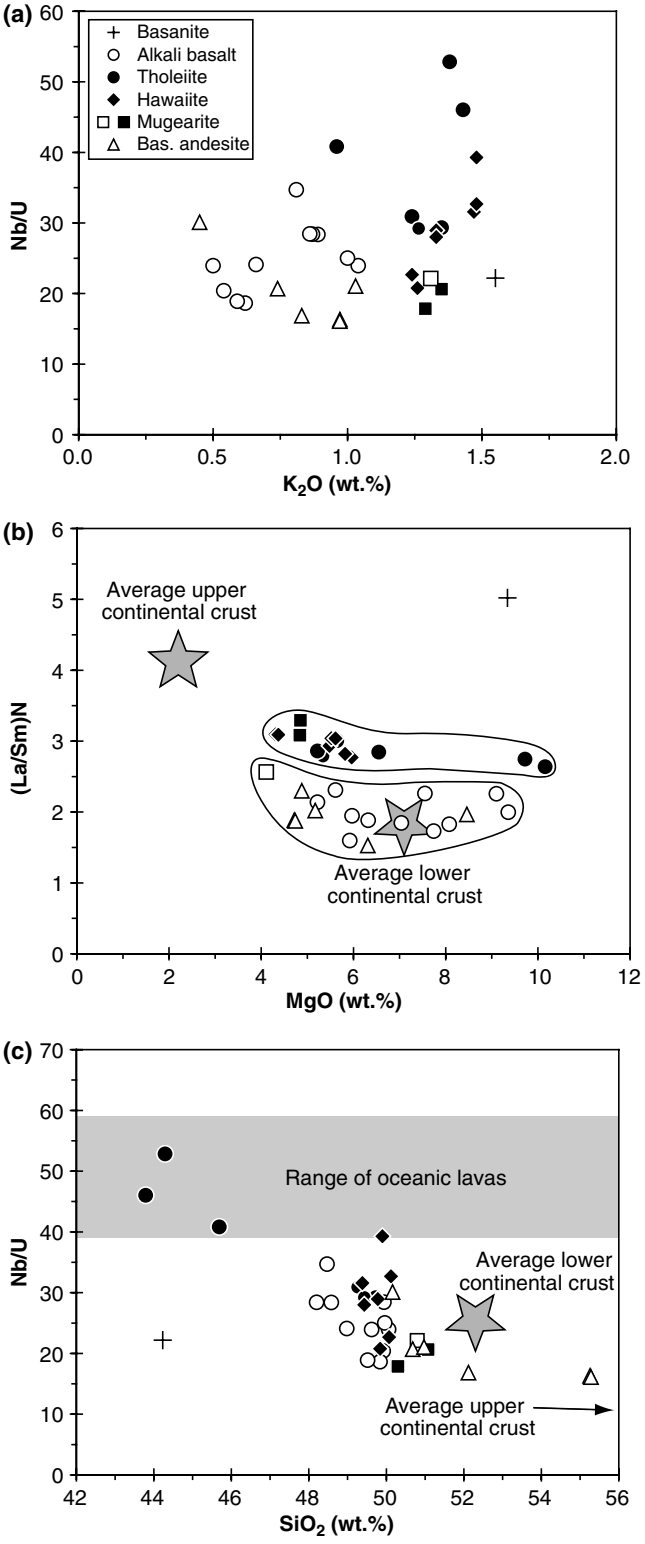

Fig. 5 Variation of **a** K_2O versus Nb/U, **b** chondrite-normalized La/Sm [$(La/Sm)_N$] versus MgO, and **c** Nb/U versus SiO_2 for the NW Syrian lavas. Note that the lavas show no correlation between K_2O and Nb/U, that the high-P lavas have higher $(La/Sm)_N$ and that both lava series show a negative correlation of Nb/U with SiO_2. The *gray field* displays the variation of Nb/U in oceanic lavas (Hofmann et al. 1986). Average continental crustal compositions of lower and upper crust are from Rudnick and Fountain (1995)

TiO_2 concentrations are negatively correlated with MgO, whereas a positive correlation is shown by the high-P group samples.

The compatible trace elements such as Cr and Ni correlate positively with MgO and Cr contents of the

high-P group samples decrease sharply below 6 wt% MgO (Fig. 4a, b).

The high-P group samples are enriched in highly incompatible elements and, for example, Nb concentrations are on average twice as high in high-P lavas compared to the low-P group (Fig. 4c). Samples of the high-P group also have chondrite-normalized La/Sm $[(La/Sm)_N]$ ratios >2.5. In contrast, the low-P lavas have $(La/Sm)_N$ generally <2.5 (Fig. 5b). Nb/U ratios of the sample suite from NW Syria range from values typical of oceanic basalts (Hofmann et al. 1986) which were not contaminated with continental crustal material to values characteristically of average continental lower crust (Nb/U = 25) and also show a trend to low Nb/U ratios as representative of continental upper crustal rocks (Nb/U = 8.93) (Rudnick and Fountain 1995). The Nb/U ratios correlate negatively with SiO_2 (Fig. 5c). Most of the primitive samples yield high Nb/U ratios and have low SiO_2 contents. In contrast, the most evolved lavas of the two groups, i.e., the basaltic andesites and the mugearites, with high SiO_2 concentrations, show low Nb/U and high $(La/Sm)_N$ ratios trending to upper continental crustal compositions (Figs. 5, 6).

Due to the young age of the NW Syrian lavas (<12 Ma) (Krienitz et al., unpublished data) age-corrections of the measured isotope ratios are insignificant and were not performed. $^{87}Sr/^{86}Sr$ and $^{143}Nd/^{144}Nd$ compositions define a negative linear trend (Fig. 7a) and basaltic samples of both groups have lower Sr and higher Nd isotopic compositions compared to the evolved lavas. The NW Syrian basalts have higher $^{87}Sr/^{86}Sr$ for a given $^{143}Nd/^{144}Nd$ relative to rocks from the Arabian lithospheric mantle and lavas from Saudi

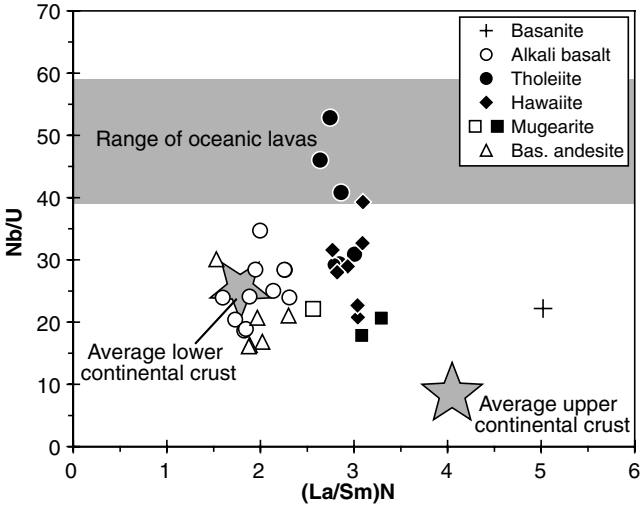

Fig. 6 Plot of $(La/Sm)_N$ versus Nb/U showing different trends for the two lava groups. The range of Nb/U in oceanic lavas (*gray field*) is from Hofmann et al. (1986). Note that the high-P lavas show a trend from uncontaminated magmas toward the average composition of the upper continental crust whereas the lower crust has a very high Nb/U. Average continental crustal compositions of lower and upper crust are from Rudnick and Fountain (1995)

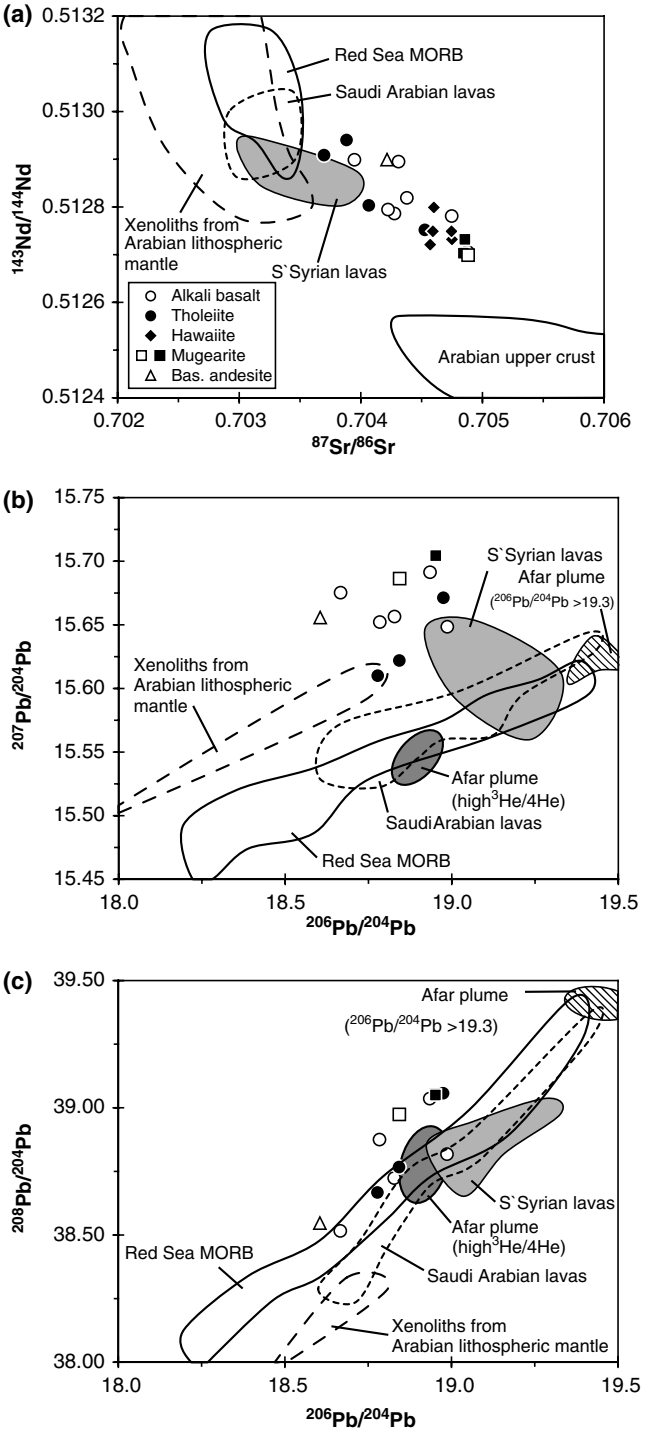

Fig. 7 Diagrams of **a** $^{87}Sr/^{86}Sr$ versus $^{143}Nd/^{144}Nd$, **b** $^{206}Pb/^{204}Pb$ versus $^{207}Pb/^{204}Pb$, and **c** $^{206}Pb/^{204}Pb$ versus $^{208}Pb/^{204}Pb$ for the NW Syrian samples compared with Arabian crustal data, clinopyroxene analyses representative of Arabian lithospheric mantle, lavas from the Red Sea region and Saudi Arabia, and with lava compositions which are related to two different Afar mantle plume components (i.e., high $^3He/^4He$ lavas and lavas with $^{206}Pb/^{204}Pb > 19.3$). *Data sources*: Arabian lithospheric mantle: Altherr et al. (1990), Henjes-Kunst et al. (1990), Blusztajn et al. (1995); Red Sea: Dupré et al. (1988), Eissen et al. (1989), Schilling et al. (1992); Saudi Arabia and southern Syria: Bertrand et al. (2003); Arabian crustal samples Hegner and Pallister (1989), Jarrar et al. (2003); Afar mantle plume: Marty et al. (1996), Pik et al. (1999), Bertrand et al. (2003)

Arabia and the Red Sea. Compared to the intraplate lavas from southern Syria the investigated sample suite lies on a steeper linear trend in the Sr and Nd isotopes extending toward the compositions of upper crustal samples from Jordan (Jarrar et al. 2003) and Saudi Arabia (Hegner and Pallister 1989) (Fig. 7a). The Pb isotope compositions of the high-P samples appear to lie on trends of increasing $^{207}Pb/^{204}Pb$ and $^{208}Pb/^{204}Pb$ with increasing $^{206}Pb/^{204}Pb$ whereas the low-P samples from NW Syria show no clear trend (Fig. 7b, c). The NW Syrian lavas trend toward the Saudi Arabian lavas with low $^{206}Pb/^{204}Pb$ of about 18.6. The $^{206}Pb/^{204}Pb$ and $^{208}Pb/^{204}Pb$ compositions of the NW Syrian samples overlap with the compositions of magmas from the Red Sea but lie outside the range representative for the Arabian lithospheric mantle (Fig. 7c). The NW Syrian lavas have higher Sr isotope ratios for a given $^{206}Pb/^{204}Pb$ compared to the Saudi Arabian and Red Sea lavas and to isotopic compositions of the Arabian lithospheric mantle (Fig. 8a). Similarly, most of the NW Syrian lavas have lower Nd isotope ratios for a given $^{206}Pb/^{204}Pb$, even though the most primitive samples partly overlap with the Saudi Arabian lavas. The NW Syrian sample suite appears to trend to upper crustal compositions and only the high-P lavas form a negative trend (Fig. 8b). The investigated samples exhibit a negative correlation between Pb/Nd and $^{143}Nd/^{144}Nd$ as well as a negative correlation between Nb/U and $^{87}Sr/^{86}Sr$ ranging between oceanic basaltic and crustal compositions (Fig. 9a, b). With respect to the $(La/Sm)_N$ ratios the lavas within each group display a slightly negative correlation with their isotopic composition (Fig. 9c).

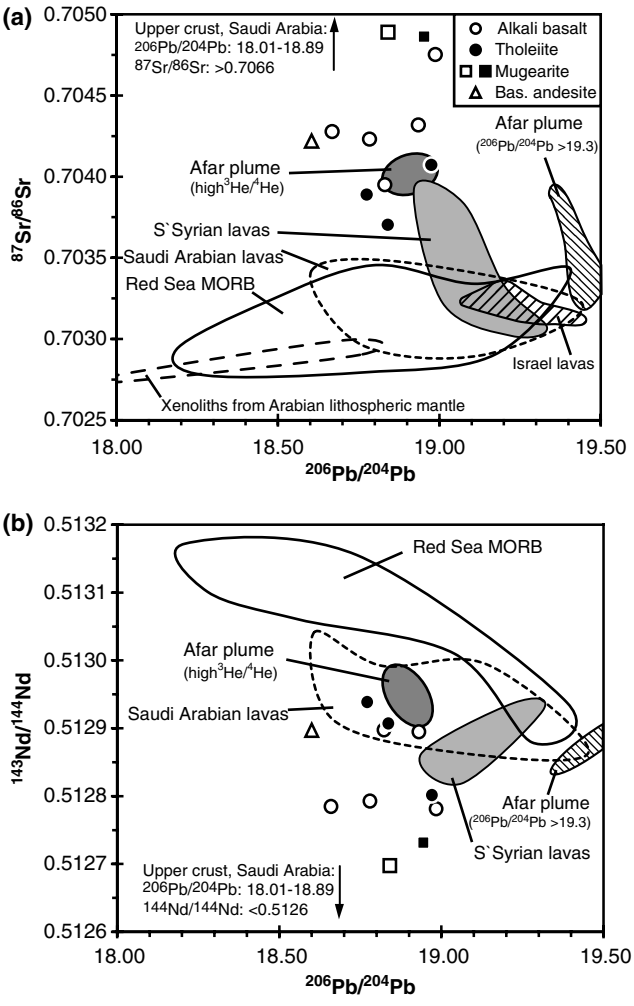

Fig. 8 Diagrams of **a** $^{206}Pb/^{204}Pb$ versus $^{87}Sr/^{86}Sr$, and **b** $^{206}Pb/^{204}Pb$ versus $^{143}Nd/^{144}Nd$ for the investigated NW Syrian samples. Additionally shown is a field of lavas from Israel. *Data source*: Stein and Hofmann (1992); other fields and data sources as in Fig. 7

Discussion

Fractional crystallization and depths of stagnation of the NW Syrian magmas

Primitive, mantle derived magmas in equilibrium with mantle olivine have Mg-numbers of 0.68–0.72 and Ni concentrations in the range of 300–500 ppm (Frey et al. 1978). Although some tholeiites and alkali basalts from NW Syria have relatively primitive Mg-numbers, ranging from 0.65 to 0.60, and Ni concentrations of about 300 ppm (Table 2), most of the rocks show lower values. The decreasing MgO contents in combination with decreasing Ni and Cr contents (Fig. 4a, b) imply crystal fractionation of olivine, clinopyroxene, and spinel. However, the different incompatible element compositions (Fig. 4c) and especially the different $(La/Sm)_N$ (Fig. 5b) of the high-P and the low-P lava series indicate that both groups formed from different parental magmas and cannot be related by fractional crystallization. The observed range of MgO contents within each lava series suggests that each series roughly lies along one liquid line of descent and the lavas from each rock suites are most likely related by crystal fractionation processes. Olivine and clinopyroxene extraction causes the increase in Al_2O_3 (Fig. 3d) and the positive correlation of CaO/Al_2O_3 ratios with decreasing MgO (not shown) in the residual melt. The increasing SiO_2 and decreasing Cr at MgO 6 wt% suggests increasing spinel fractionation. Positive Sr anomalies [average $Sr/Sr^* = 1.34$; $Sr/Sr^* = Sr_N/SQR\ (Pr_N \times P_N)$], the lack of Eu anomalies [average $Eu/Eu^* = 1.00$; $Eu/Eu^* = Eu_N/SQR\ (Sm_N \times Gd_N)$], and constantly rising Al_2O_3 concentrations indicate that low pressure plagioclase fractionation did not play a major role in the petrogenesis of the NW Syrian magmas.

In order to estimate the pressure–temperature range of the crystallization of the NW Syrian lavas we use the clinopyroxene-melt thermobarometer of Putirka et al. (1996). The high-P group samples reveal pressure conditions between 0.7 and 0.4 GPa corresponding to depths of 25–14 km using a crustal density of 2.8 g/cm^3, but mostly give a range of 0.6–0.5 GPa (21–18 km) for

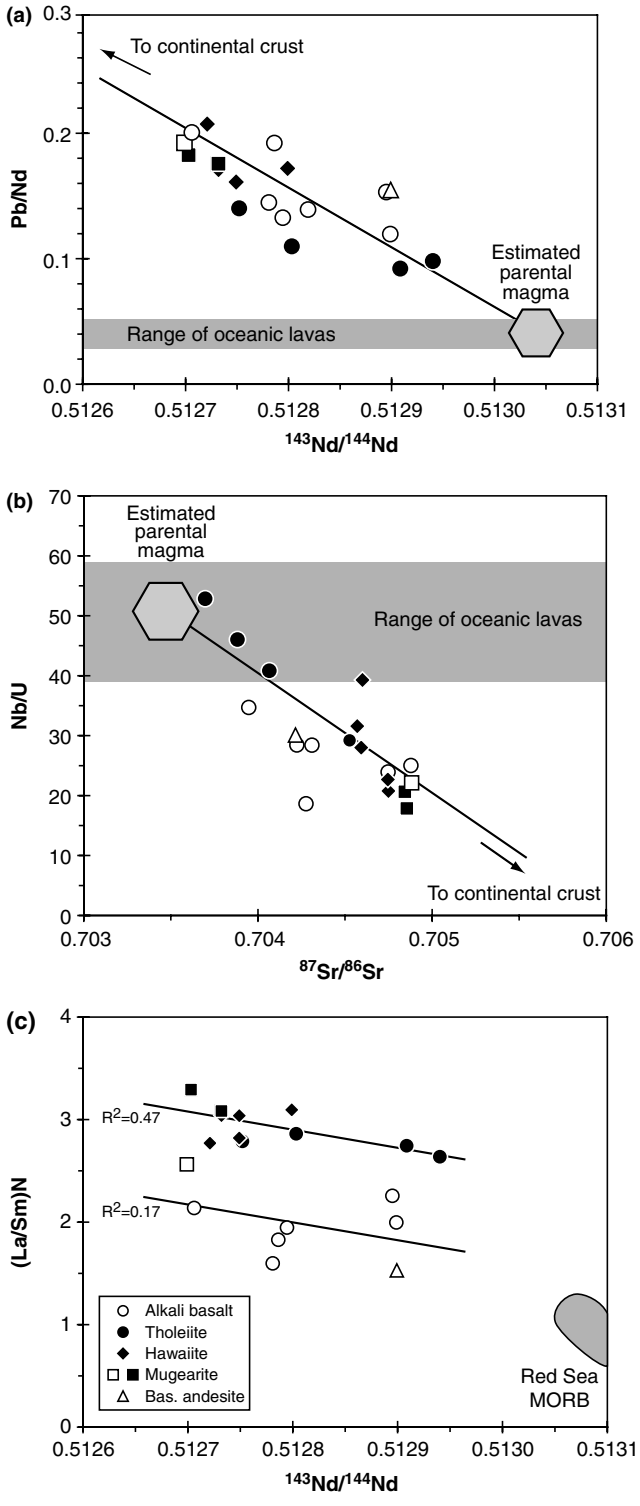

Fig. 9 Plots of **a** $^{143}Nd/^{144}Nd$ versus Pb/Nd, **b** $^{87}Sr/^{86}Sr$ versus Nb/U, and **c** $^{143}Nd/^{144}Nd$ versus $(La/Sm)_N$. The compositions of the uncontaminated magmas can be estimated based on the nearly constant Pb/Nd and Nb/U ratios in mantle melts (Hofmann et al. 1986; Mahoney et al. 1994). Data sources for Red Sea MORB as in Fig. 6

the crystallization process. In contrast, clinopyroxene crystallization of the low-P group takes place at shallower depths of about 0.3 GPa (~11 km). Thus, the crystallization pressure conditions indicate that the high-P group magmas stagnated deeper in the crust than the low-P group but both magma series crystallized within the uppermost ~20 km of the continental crust but below the sediment cover (~6 km thickness). These estimates are similar to observations made by Baker et al. (1997) for lavas from western Yemen which have undergone polybaric fractionation of olivine, clinopyroxene, plagioclase, and Fe-Ti oxides.

For quantitative modeling of fractionation processes the software MELTS from Ghiorso and Sack (1995) was used and the results for two parental magmas are shown in Table 4 and Fig. 3. Although the low-P lava series can be matched reasonably well, the fit of the model to the high-P lava series is poor due to the scatter of the lavas within this group. According to the MELTS model the most evolved lavas from the low-P group have fractionated about 22% clinopyroxene and 8% plagioclase. In contrast, the high-P group has fractionated about 37% clinopyroxene, 6% olivine, 3% plagioclase, and 7% spinel to evolve from an alkali basalt to a mugearite (Table 4). The removal of plagioclase as suggested by the model do not agree with the observed positive Sr anomalies and the lack of Eu anomalies in lavas indicating that other processes in addition to fractional crystallization have affected the composition of lavas. However, the model results are consistent with the mineral phases observed in thin sections with the exception of olivine which occurs in larger amounts than suggested by the model. The fractionation of olivine at even greater depth may account for the generation of the primitive alkali basalts the compositions of which were used in the MELTS software to model the fractional crystallization trends of the Syrian lavas. The results for high-P lavas are similar to Pleistocene volcanic rocks from Israel that have undergone up to 30% of mainly clinopyroxene and olivine fractionation and only minor amounts of other phases (Weinstein et al. 1994).

Crustal contamination

Both groups of the NW Syrian lavas show similar but variable ranges of Sr and Nd isotope ratios and highly incompatible element ratios versus isotopes implying that more than one end member is involved in magma genesis (Figs. 7a, 9). The presence of quartz xenocrysts in some of the basaltic lavas suggests a reaction of the ascending magmas with country rocks. Hofmann et al. (1986) showed that oceanic magmas have Nb/U ratios of 49 ± 10 implying that this range represents the Nb/U of the upper mantle. In contrast, the average upper continental crust has a Nb/U of 9 and the lower crust of 25 (Rudnick and Fountain 1995). The decrease of the Nb/U ratios observed during magmatic differentiation of the NW Syrian magmas cannot be achieved by crystal fractionation only because the removal of mineral phases would not fractionate these elements. Consequently, the negative correlation between SiO_2 and Nb/U

Table 4 Fractional crystallization modeling for lavas of NW Syria using MELTS

	Input values			Initial values recalculated by MELTS	
	Low P-group	High P-group		Low P-group	High P-group
T range (°C)	1,300–850	1,300–850	$T_{liquidus}$ (°C)	1,239	1,268
P (kbar)	3	3	P (kbar)	3	3
$\log_{(10)} fO_2$	0	0	$\log_{(10)} fO_2$	−6.87	−6.57
QFM	+1	+1	QFM	+1	+1
SiO_2 (wt%)	49.62	43.79	SiO_2 (wt%)	50.57	45.78
TiO_2 (wt%)	1.68	2.50	TiO_2 (wt%)	1.71	2.61
Al_2O_3 (wt%)	13.34	12.30	Al_2O_3 (wt%)	13.59	12.86
FeO^T (wt%)	10.45	11.50	FeO^T (wt%)	10.88	12.29
MnO (wt%)	0.14	0.17	MnO (wt%)	0.14	0.18
MgO (wt%)	8.66	10.16	MgO (wt%)	8.83	10.62
CaO (wt%)	9.54	10.49	CaO (wt%)	9.72	10.97
Na_2O (wt%)	2.80	2.34	Na_2O (wt%)	2.85	2.45
K_2O (wt%)	0.64	1.00	K_2O (wt%)	0.65	1.05
P_2O_5 (wt%)	0.23	0.35	P_2O_5 (wt%)	0.23	0.37
H_2O (wt%)	0.50	0.50	H_2O (wt%)	0.51	0.52
CO_2 (wt%)	0.30	0.30	CO_2 (wt%)	0.31	0.31
Total (wt%)	97.90	95.40	Total (wt%)	99.99	100.01

Low P-group Fractionated phases at		Phase	wt%	Composition
T	1,119°C	cpx	21.56	Di 29, En 22, He 22, Jd 3.0
MgO	3.92 wt%	plag	8.43	Ab 38, An 61, Sa 1.1
		Total	29.99	

High P-group Fractionated phases at		Phase	wt%	Composition
T	1,108°C	ol	6.28	Fo 79
MgO	3.67 wt%	cpx	36.96	Di 36, En 18, He 17, Jd 3.1
		plag	2.93	Ab 37, An 61, Sa 1.7
		spinel	6.86	Usp 31, Mt 47, Sp 5.1
		Total	53.03	

indicates the crustal contamination of the magmas (Fig. 5c). Assimilation of continental crust is also indicated by the isotopic compositions of the lavas (Fig. 7) and the trends of Pb/Nd versus $^{143}Nd/^{144}Nd$ and Nb/U versus $^{87}Sr/^{86}Sr$ (Fig. 9a, b). Especially the most evolved samples exhibit Nd and Sr isotope compositions clearly outside the fields of any mantle source in the region but trend toward the composition of the upper continental crust (Figs. 7a, 8). The observed correlations between Pb/Nd and Nb/U ratios and isotopic compositions throughout the differentiation trends are interpreted as the combined effects of assimilation and fractional crystallization (AFC) in the NW Syrian magmas (Fig. 9a, b). However, even though the AFC processes can also account for the observed negative correlation between Nd isotopes and $(La/Sm)_N$ within each group of lavas (Fig. 9c), the differences between the high-P and the low-P group cannot be due to the contamination but must have formed during the magma genesis in the mantle. Because both the high-P and the low-P group share an isotopically similar mantle source the observed differences in incompatible element enrichment between both groups are caused either by variable degrees of partial melting or by a relatively young depletion or enrichment event of parts of this source which did not affect the radiogenic isotopes (Figs. 3, 4, 5, 9).

Based on Sr and Nd isotopic compositions of the NW Syrian lavas AFC-processes were modeled using the energy-constrained assimilation-fractional crystallization (EC-AFC) model of Spera and Bohrson (2001). Because the clinopyroxene-melt thermobarometry indicates magma stagnation at upper crustal levels, the assimilants were most likely the upper crustal rocks. The composition of the assimilant with high $(La/Sm)_N$, Pb/Nd, and low Nb/U also supports an upper crustal, i.e., granitic component rather than mafic lower crustal material (Figs. 6, 9). Thus, in the model we used assimilant compositions similar to upper crustal rocks and an average Sr and Nd isotopic composition of hypothetical parental magmas which can be estimated on the basis of the relatively constant Pb/Nd and Nb/U ratios in mantle melts (Hofmann et al. 1986; Mahoney et al. 1994) and EC-AFC parameters for the ''standard'' upper crustal case as given by Bohrson and

Spera (2001) (Table 5, Fig. 9a, b). Figure 10 shows that the isotopic and incompatible element variations of the two different Syrian lava groups can be modeled by the EC-AFC processes using two different parental magma compositions. These two parental magmas have approximately similar Sr and Nd isotopic compositions but very different Sr and Nd concentrations, i.e., the high-P group is much more enriched than the low-P group lavas. The model indicates that the evolved high-P group lavas have fractionated between 40 and 60% and have assimilated between <5 and about 25% of upper crustal material but suggests higher assimilation rates of up to 45% on the basis of Nd versus $^{143}Nd/^{144}Nd$ (Fig. 10b). In contrast, only $<10\%$ assimilation and 45–50% fractionation are needed to produce the isotopic composition of the low-P group lavas (Fig. 10). The results of the EC-AFC modeling are in accordance with the quantitative modeling of the crystallization processes using MELTS (Table 4, Fig. 3), although the results of the EC-AFC calculations are slightly higher for the low-P group samples. The contamination of an alkali basalt with ~48 wt% SiO_2 by 45% of upper crustal material with ~68 wt% SiO_2 (Jarrar et al. 2003) produces lava compositions with about 63 wt% SiO_2. Thus, the modeled assimilation rates of 45% appear too high for the high-P group, because only lavas with silica contents <56 wt% can be observed in NW Syria (Fig. 2). However, an exact quantification of AFC processes is limited due to: (1) the unknown incompatible element concentrations of the parental magmas, (2) the heterogeneous geochemical nature of the crust, and (3) the uncertainties of the bulk distribution coefficients of Sr during assimilation and fractional crystallization.

Deep seismic refraction data of El-Isa et al. (1987) and geochemical studies of crustal rocks and xenoliths (Nasir 1992; Nasir and Safarjalani 2000; Jarrar et al. 2003) have shown that the upper crust in NW Arabia consists of mafic and intermediate to presumably felsic rocks while the lower crust below 20 km depth is more mafic. Since magmas of the two NW Syrian groups stagnated in the upper crust at maximum depths of <20 km, it is likely that the magmas have assimilated upper crustal material. Although the EC-AFC model yields realistic results for the assimilation of upper crustal rocks, the possibility to generate low-P group samples by addition of a felsic crustal component to primitive high-P group magmas can be excluded. For example, the assimilation of felsic upper crustal rocks (e.g., granitic crust of southern Jordan; Jarrar et al. 2003) could account for the relatively high SiO_2 concentrations in the low-P group lavas (Fig. 3b), but the K contents of the melts from granitic upper crust (>3.4 wt% K_2O, Jarrar et al. 2003) would lead to high K_2O concentrations in melts whereas the low-P lavas have relatively low K contents (Fig. 3h). However, concerning lavas with alkali basaltic and tholeiitic compositions, the results of this study gave similar masses of assimilation for the NW Syrian magmas compared to basanites and alkali basalts of Jordan, which have assimilated up to 20% of upper crust (Shaw et al. 2003).

Table 5 Input parameters for EC-AFC computations

Thermal parameters	T (°C)		
Magma liquidus temperature	1,300	Isobaric specific heat of magma	1,484 J/kg K
Magma initial temperature	1,300	Isobaric specific heat of assimilant	1,370 J/kg K
Assimilant liquidus temperature	1,000	Crystallization enthalpy	396,000 J/kg
Assimilant initial temperature	350	Fusion enthalpy	270,000 J/kg
Solidus temperature	900		
Equilibration temperature	1,030		

Compositional parameters	Sr	Nd
Magma A		
Magma initial concentration (ppm)	600	15
Magma isotope ratio	0.7035	0.51305
Magma trace element distribution coefficient	0.7	0.25
Magma B		
Magma initial concentration (ppm)	330	7
Magma isotope ratio	0.7035	0.51305
Magma trace element distribution coefficient	0.7	0.25
Assimilant		
Assimilant initial concentration (ppm)	63	22
Assimilant isotope ratio	0.7220	0.5123
Assimilant trace element distribution coefficient	0.08	0.25

Computations were performed using the computer program EC-AFC as cited in Spera and Bohrson (2001)

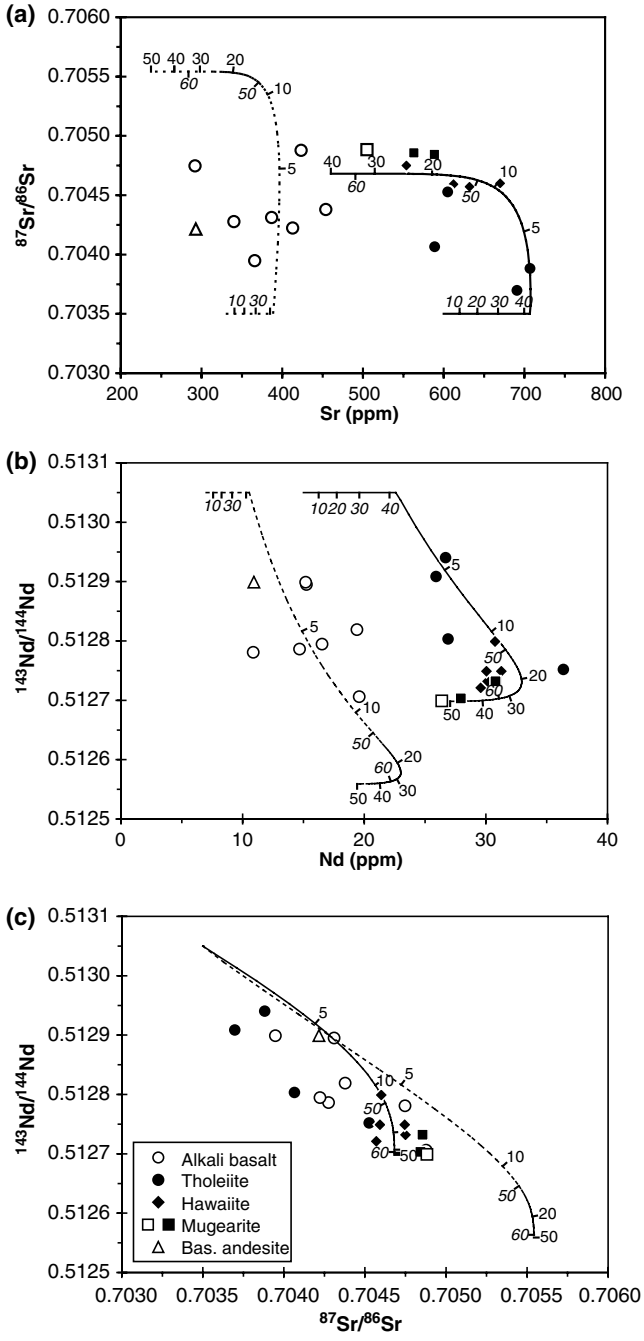

Fig. 10 Results for EC-AFC modeling. **a** Sr versus $^{87}Sr/^{86}Sr$, **b** Nd versus $^{143}Nd/^{144}Nd$ and **c** $^{87}Sr/^{86}Sr$ versus $^{143}Nd/^{144}Nd$. *Continuous lines* refer to calculated curves for high-P group samples (Magma A, Table 5) and *dotted lines* to low-P group samples (Magma B, Table 5) using the software program EC-AFC of Spera and Bohrson (2001). *Italic numbers* give the amount of fractional crystallization and *other numbers* the percentage of anatectic melt assimilated

The mantle sources of the NW Syrian magmas

Sr and Nd isotope ratios and highly incompatible element ratios versus isotope ratios of both lava series define similar trends implying that the sources of the high-P and low-P magmas must have been similar in terms of isotopic and highly incompatible element ratios (Figs. 7a, 9a, b). It is suggested that the least contaminated high-P lavas lie close to the isotopic composition of the mantle source and on the basis of the contamination (AFC) trends (Figs. 7a, 9, b) we suggest that this source must have $^{87}Sr/^{86}Sr = 0.7035$, $^{143}Nd/^{144}Nd = 0.51305$, and $^{206}Pb/^{204}Pb = 18.6$ and thus resembles the depleted mantle component C2 in the Ethiopian lavas studied by Pik et al. (1999). The voluminous volcanism in the Red Sea region probably reflects the presence of the Afar deep mantle plume which has also been detected by seismic tomography studies (Daradich et al. 2003). Two different sources appear to reside in this plume and have been observed in lavas in NE Africa and on the Arabian Peninsula; (1) an ocean island basalt-like mantle component in high-Ti magmas of the Ethiopian flood basalt province with high $^{3}He/^{4}He$ ratios (Marty et al. 1996; Pik et al. 1999), and (2) a source with $^{206}Pb/^{204}Pb$ isotope ratios >19.3 which occurs in lavas from Saudi Arabia (Bertrand et al. 2003) and the southern Red Sea and Gulf of Aden (Schilling et al. 1992). Both of these plume sources are different from the source of the NW Syrian lavas and thus there is no evidence for an inflow of Afar plume material from the south as has been suggested by Camp and Roobol (1989) (Figs. 7, 8). Stein and Hofmann (1992) proposed that the volcanism in Israel may be the result of lithospheric extension and melting of a fossil plume head beneath the base of the lithosphere. However, the lavas from Israel have lower $^{87}Sr/^{86}Sr$ and more radiogenic $^{206}Pb/^{204}Pb$ ratios compared to NW Syrian lavas implying that such a fossil plume component does not contribute to the mantle source of Syrian lavas (Fig. 8a). In terms of Nd and Pb isotope compositions the source of the NW Syrian magmas lies at the relatively enriched end of the Red Sea MORB field but it has higher $^{87}Sr/^{86}Sr$ than Red Sea MORB (Figs. 7, 8). Consequently, it may represent an enriched component of the lower part of the continental thermal boundary layer in accordance with Pik et al. (1999), or the asthenosphere beneath NW Syria contains enriched portions with a higher Sr isotope composition than Red Sea MORB. Interestingly, higher $^{87}Sr/^{86}Sr$ for a given $^{143}Nd/^{144}Nd$ is observed in basalts from the northernmost Red Sea deeps compared to MORB from the southern Red Sea (Haase et al. 2000), indicating an increasing $^{87}Sr/^{86}Sr$ in the upper mantle toward the northern Red Sea. The lavas from Red Sea MORB with the lowest $^{143}Nd/^{144}Nd$ have $(La/Sm)_N$ of up to 1.3 (Fig. 9c) suggesting that they formed from a source with only little depletion or even enrichment relative to primitive mantle (Haase et al. 2000). We propose that the NW Syrian magmas may have formed from relatively enriched portions of the asthenosphere beneath this region.

Magma generation and its causes beneath NW Syria

P_2O_5 as well as Nb concentrations are twice as high in the high-P group compared to lavas of the low-P group

(Figs. 3, 4), suggesting that low-P lavas may have formed from a mantle source which was depleted in incompatible elements relative to the high-P group. However, in the volcanic succession sampled near Bulbul the high-P lavas lie above low-P lavas implying that increasing depletion of the mantle source with time cannot explain the generation of the magmas (Fig. 11). Rather, the chemical evolution of the two compositional groups at Bulbul suggests that the observed differences are controlled by variable degrees of partial melting. Because the enrichment of incompatible elements increases by a factor of two the decrease of partial melting must be of the order of 50%. Since garnet has a large distribution coefficient for heavy rare earth elements (HREE), melting of a garnet-bearing mantle source would fractionate those from light rare earth elements (LREE) resulting in higher LREE/HREE ratios (e.g., Ce/Yb) compared to middle REE/HREE ratios (e.g., Sm/Yb). Therefore, the variations of the REE ratios shown in Fig. 12 indicate that melting occurred in the garnet stability field. Assuming an enriched mantle source the early low-P magmas can be generated by about 8% of melting and the younger high-P lavas by about 4% melting of an identical source (Fig. 12).

The SiO_2 contents of uncontaminated primitive magmas for the high-P and low-P lava series are 44 and 48 wt%, respectively (Figs. 3b, 5b). The SiO_2 content of magma is indicative for pressure conditions during partial melting (Hirose and Kushiro 1993) and we estimate average melting pressures on the basis of the algorithm developed by Haase (1996). According to this model melting of NW Syrian magmas occurred at pressures of about 3.9 GPa for high-P lavas and at about 2.2 GPa for low-P lavas, corresponding to average melting depths of about 120 and 70 km, respectively. Based on xenolith data McGuire and Bohannon (1989) place the lithosphere–asthenosphere boundary in W Arabia at a depth of about 75 km. Assuming a similar lithospheric thickness for NW Syria, the calculated depths of the Syrian lavas indicate that first stage melting occurred at the lower boundary of the lithosphere and during the second stage (high-P group lavas) partial melting occurred in the asthenosphere. The lava succession at Bulbul suggests that during the first melting stage relatively large degree melts were formed in the shallow mantle and during the second stage lower degree

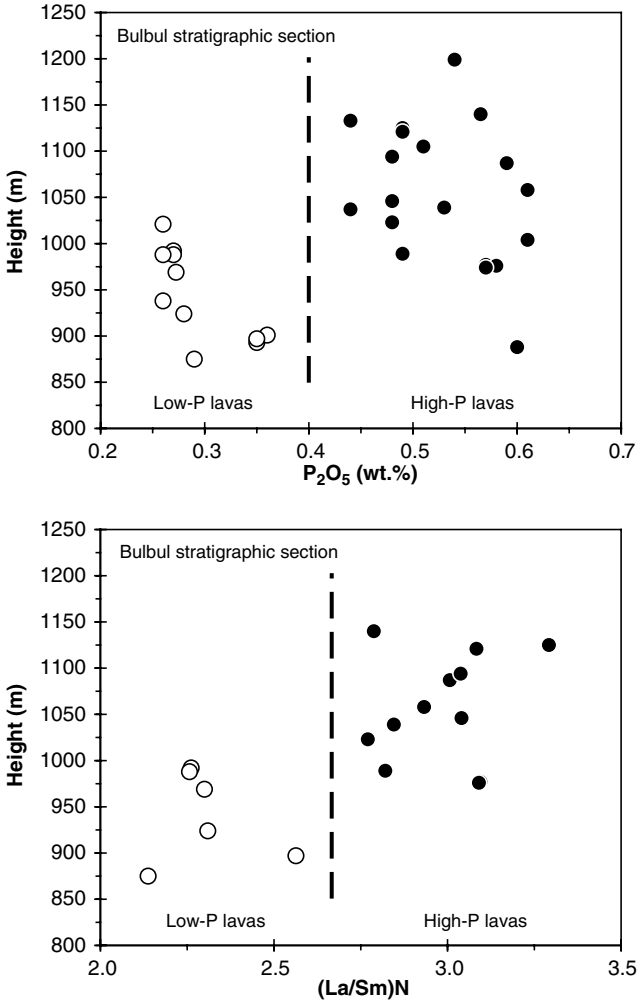

Fig. 11 Plots of **a** P_2O_5 versus height and **b** $(La/Sm)_N$ versus height for the Bulbul lava succession. The two lava series are separated by a soil horizon suggesting that there was a major break in the volcanism between the eruption of the two series

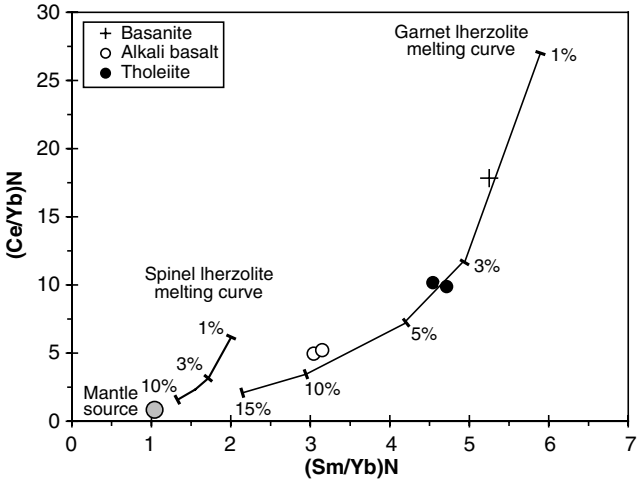

Fig. 12 Diagram of chondrite-normalized Sm/Yb and Ce/Yb ratios showing the primitive uncontaminated lavas of each group and a melting curve for non-modal fractional melting of garnet and spinel lherzolite. Garnet lherzolite composition: 0.598 olivine, 0.076 clinopyroxene, 0.211 orthopyroxene, 0.115 garnet. Melting proportions of garnet lherzolite: 0.05 olivine, 0.3 clinopyroxene, 0.2 orthopyroxene, 0.45 garnet. Spinel lherzolite composition: 0.578 olivine, 0.119 clinopyroxene, 0.27 orthopyroxene, 0.033 spinel. Melting proportions of spinel lherzolite: 0.10 olivine, 0.50 clinopyroxene, 0.27 orthopyroxene, 0.13 spinel. Enriched mantle source composition (relative to the mantle source composition of average mid-ocean ridge basalts from Hofmann 1988): Ce 1.56 ppm, Sm 0.39 ppm, and Yb 0.41. Distribution coefficients used are from Kelemen et al. (1993) and Johnson (1998). *Numbers* give the degree of melting and chondrite values are from McDonough and Sun (1995)

melts were produced at greater depths. At a normal potential mantle temperature of 1,280°C the lithosphere should be stretched by a factor of ~2 to generate partial melts from dry mantle (McKenzie and Bickle 1988). However, there are no indications for extensional processes during the magmatic activity in NW Syria and hence volcanism cannot be a consequence of lithospheric extension. Several of the NW Syrian volcanic units, like the Bulbul lavas, belong to a belt of alkaline volcanoes extending across the Eastern Anatolian Fault zone (Fig. 1). Keskin (2003) suggested that this volcanism may be due to the slab-breakoff which occurred at 11–10 Ma ago and thus coincides with the eruption of the Bulbul lavas (Krienitz et al., unpublished data) (Fig. 13). Asthenospheric upwelling above the sinking slab could then generate melts. Magmatism caused by slab-breakoff has been suggested by Davies and von Blankenburg (1995) but these authors proposed that the hot asthenosphere upwelling leads to melting of the metasomatized lithosphere of the upper plate of a former subduction zone. This cannot be the case in NW Syria and eastern Turkey because the lavas are clearly alkaline and do not show an enrichment of the fluid-mobile elements which would be expected from lithospheric mantle above a former subduction zone. We propose that the NW Syrian magmas were formed by melting of an enriched and possibly volatile-rich portion of upwelling asthenospheric mantle which was triggered by sinking of the slab (Fig. 13). This could also explain the different depths of melting because upwelling will proceed to greater depths with time as the slab sinks deeper and deeper into the mantle.

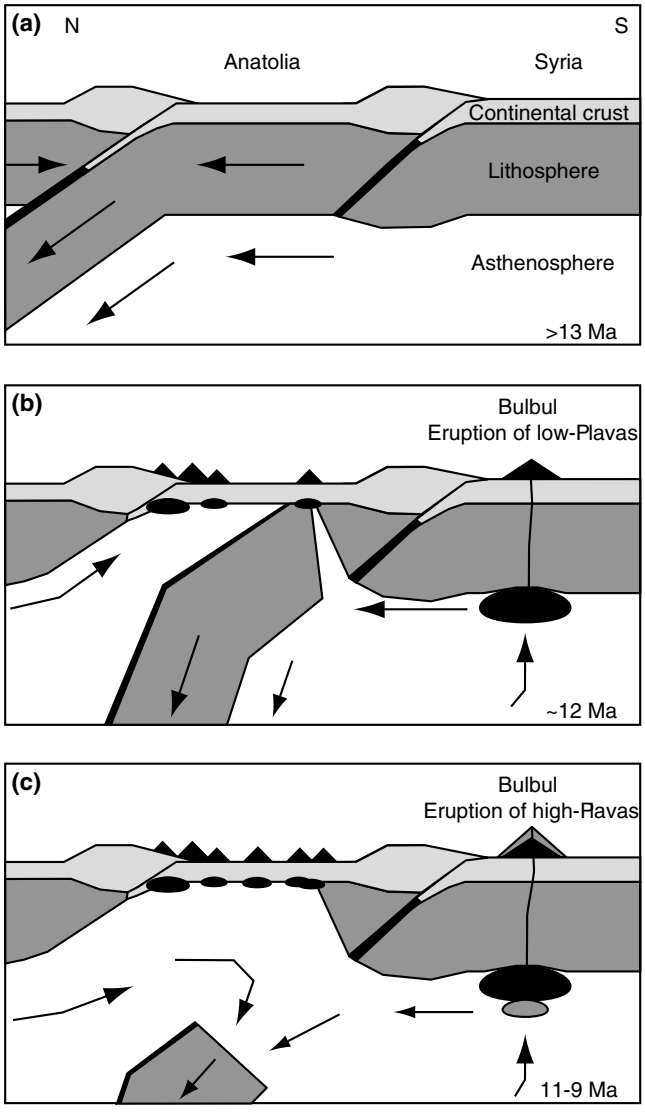

Fig. 13 Schematic cross sections showing magma generation in NW Syria and Eastern Anatolia by slab break-off. **a** The tectonic situation before the slab break-off process commences. **b** Steepening and rifting of the subducting plate cause upwelling of the surrounding asthenosphere. At ~12 Ma the return flow of hot asthenosphere under northwestern Arabia induces melt generation in the asthenosphere in depths of about 70 km producing the low-P lavas. **c** As the slab sinks deeper into the mantle a deep return flow of asthenosphere leads to melt production in depths of about 120 km generating the high-P lavas between 11 and 9 Ma

Acknowledgments We thank D. Garbe-Schönberg for the the ICP-MS and A. Weinkauf for performing the XRF analyses. P. Appel and B. Mader are thanked for their help with the microprobe analyses. M.-S.K. thanks H. Baier for her help with the sample preparation for isotopic analysis and Zaghier Ali for his help during field work. This study is part of M.-S.K.'s dissertation and was funded by the Deutsche Forschungsgemeinschaft under grant HA 2568/5.

References

Aitcheson SJ, Forrest AH (1994) Quantification of crustal contamination in open magmatic systems. J Petrol 35:461–488

Altherr R, Henjes-Kunst F, Baumann A (1990) Asthenosphere versus lithosphere as possible sources for basaltic magmas erupted during formation of the Red Sea; constraints from Sr, Pb and Nd isotopes. Earth Planet Sci Lett 96:269–286

Baker JA, Menzies MA, Thirlwall MF, Macpherson CG (1997) Petrogenesis of quaternary intraplate volcanism, Sana'a, Yemen; implications for plume-lithosphere interaction and polybaric melt hybridization. J Petrol 38:1359–1390

Bertrand H, Chazot G, Blichert-Toft J, Thoral S (2003) Implications of widespread high-μ volcanism on the Arabian Plate for Afar mantle plume and lithosphere composition. Chem Geol 198:47–61

Best JA, Barazangi M, Al SD, Sawaf T, Gebran A (1990) Bouguer gravity trends and crustal structure of the Palmyride mountain belt and surrounding northern Arabian Platform in Syria. Geology 18:1235–1239

Blusztajn J, Hart SR, Shimizu N, McGuire AV (1995) Trace-element and isotopic characteristics of spinel peridotite xenoliths from Saudi Arabia. Chem Geol 123:53–65

Bohannon RG, Naeser CW, Schmidt DL, Zimmermann RA (1989) The timing of uplift, volcanism, and rifting peripheral to the Red Sea; a case for passive rifting? J Geophys Res 94:1683–1701

Bohrson WA, Spera FJ (2001) Energy-constrained open-system magmatic processes; II. Application of energy-constrained assimilation-fractional crystallization (EC-AFC) model to magmatic systems. J Petrol 42: 1019–1041

Camp VE, Roobol MJ (1989) The Arabian continental alkali basalt province; Part I. Evolution of Harrat Rahat, Kingdom of Saudi Arabia; with Suppl. Data 89–04. Geol Soc Am Bull 101:71–95

Camp VE, Roobol MJ (1992) Upwelling asthenosphere beneath western Arabia and its regional implications. J Geophys Res 97:15,255–215,271

Daradich A, Mitrovica JX, Pysklywec RN, Willett SD, Forte A, M (2003) Mantle flow, dynamic topography, and rift-flank uplift of Arabia. Geology 31:901–904

Davies JH, von Blanckenburg F (1995) Slab breakoff: A model of lithosphere detachment and its test in the magmatism and deformation of collisional orogens. Earth Plan Sci Lett 129:85–102

DePaolo DJ (1981) Trace element and isotopic effects of combined wallrock assimilation and fractional crystallization. Earth Plan Sci Lett 53:189–202

Dupré B, Blanc G, Boulegue J, Allègre CJ (1988) Metal remobilization at a spreading centre studied using lead isotopes. Nature 333:165–167

Eissen JP, Juteau T, Joron JL, Dupré B, Humler E, Al'Mukhamedov A (1989) Petrology and geochemistry of basalts from the Red Sea axial rift at 18 degrees North. J Petrol 30:791–839

El-Isa ZH, Mechie J, Prodehl C, Makris J, Rihm R (1987) A crustal structure study of Jordan derived from seismic refraction data. Tectonophysics 138(2–4):235–253

Ellam RM, Cox KG (1991) An interpretation of Karoo picrite basalts in terms of interaction between asthenospheric magmas and the mantle lithosphere. Earth Plan Sci Lett 105:330–342

Frey FA, Green DH, Roy SD (1978) Integrated models of basalt petrogenesis; a study of quartz tholeiites to olivine melilitites from south eastern Australia utilizing geochemical and experimental petrological data. J Petrol 19:463–513

Gallagher K, Hawkesworth CJ (1992) Dehydration melting and the generation of continental flood basalts. Nature 358:57–59

Garbe-Schönberg C-D (1993) Simultaneous determination of thirty-seven trace elements in twenty-eight international rock standards by ICP-MS. Geostandard Newslett 17:81–97

Ghiorso MS, Sack RO (1995) Chemical mass transfer in magmatic processes. IV. A revised and internally consistent thermodynamic model for the interpolation and extrapolation of liquid-solid equilibria in magmatic systems at elevated temperatures and pressures. Contrib Mineral Petrol 119:197–212

Haase KM (1996) The relationship between the age of the lithosphere and the composition of oceanic magmas; constraints on partial melting, mantle sources and the thermal structure of the plates. Earth Plan Sci Lett 144:75–92

Haase KM, Muehe R, Stoffers P (2000) Magmatism during extension of the lithosphere; geochemical constraints from lavas of the Shaban Deep, northern Red Sea. Chem Geol 166(3–4):225–239

Hegner E, Pallister JS (1989) Pb, Sr, and Nd isotopic characteristics of Tertiary Red Sea Rift volcanics from the central Saudi Arabian coastal plain. J Geophys Res 94:7749–7755

Henjes-Kunst F, Altherr R, Baumann A (1990) Evolution and composition of the lithospheric mantle underneath the western Arabian Peninsula; constraints from Sr-Nd isotope systematics of mantle xenoliths. Contrib Mineral Petrol 105:460–472

Hirose K, Kushiro I (1993) Partial melting of dry peridotites at high pressures; determination of compositions of melts segregated from peridotite using aggregates of diamond. Earth Plan Sci Lett 114(4):477–489

Hofmann AW (1988) Chemical differentiation of the Earth; the relationship between mantle, continental crust, and oceanic crust. Earth Plan Sci Lett 90:297–314

Hofmann AW, Jochum KP, Seufert M, White WM (1986) Nb and Pb in oceanic basalts; new constraints on mantle evolution. Earth Plan Sci Lett 79:33–45

Jarrar G, Stern RJ, Saffarini G, Al-Zubi H (2003) Late- and post-orogenic Neoproterozoic intrusions of Jordan: implications for crustal growth in the northernmost segment of the East African Orogen. Precambrian Res 123:295–319

Johnson KTM (1998) Experimental determination of partition coefficients for rare earth and high-field-strength elements between clinopyroxene, garnet, and basaltic melt at high pressure. Contrib Mineral Petrol 133:60–68

Kelemen PB, Shimizu N, Dunn T (1993) Relative depletion of niobium in some arc magmas and the continental crust; partitioning of K, Nb, La and Ce during melt/ rock reaction in the upper mantle. Earth Plan Sci Lett 120:111–133

Keskin M (2003) Magma generation by slab steepening and breakoff beneath a subduction-accretion complex: An alternative model for collision-related volcanism in Eastern Anatolia, Turkey. Geophys Res Lett 30: DOI:10.1029/2003GL018019

Kumar MR, Ramesh DS, Saul J, Sarkar D, Kind R (2002) Crustal structure and upper mantle stratigraphy of the Arabian shield. Geophys Res Lett 29: DOI:10.1029/2001GL014530

Le Bas MJ, Le Maitre RW, Streckeisen A, Zanettin BA (1986) Chemical classification of volcanic rocks based on the total alkali-silica diagram. J Petrol 27:745–750

Le Maitre RW (ed) (1989) A classification of igneous rocks and glossary of terms: Recommendations of the IUGS Subcommission on the systematics of igneous rocks, Blackwell, Oxford, p 193

Mahoney JJ, Sinton JM, Kurz MD, Macdougall JD, Spencer KJ, Lugmair GW (1994) Isotope and trace element characteristics of a super-fast spreading ridge: East Pacific rise, 13–23°S. Earth Plan Sci Lett 121:173–193

Marty B, Pik R, Gezahegn Y (1996) Helium isotopic variations in Ethiopian plume lavas; nature of magmatic sources and limit on lower mantle contribution. Earth Plan Sci Lett 144:223–237

McBride JH, Barazangi M, Best J, Al Saad D, Sawaf T, Al Otri M, Gebran A (1990) Seismic reflection structure of intracratonic Palmyride fold-thrust belt and surrounding Arabian Platform, Syria. Am Assoc Pet Geol Bull 74:238–259

McDonough WF, Sun S-s (1995) The composition of the Earth. Chem Geol 120:223–253

McGuire AV, Bohannon RG (1989) Timing of mantle upwelling; evidence for a passive origin for the Red Sea Rift. J Geophys Res 94:1677–1682

McKenzie D, Bickle MJ (1988) The volume and composition of melt generated by extension of the lithosphere. J Petrol 29(3):625–679

Nasir S (1992) The lithosphere beneath the northwestern part of the Arabian Plate (Jordan); evidence from xenoliths and geophysics. Tectonophysics 201:357–370

Nasir S, Safarjalani A (2000) Lithospheric petrology beneath the northern part of the Arabian Plate in Syria: evidence from xenoliths in alkali basalts. J Afr Earth Sci 30:149–168

Pik R, Deniel C, Coulon C, Yirgu G, Marty B (1999) Isotopic and trace element signatures of Ethiopian flood basalts; evidence for plume-lithosphere interactions. Geochim Cosmochim Acta 63:2263–2279

Ponikarov VP, Protasevich L, Maximov A, Tkachev G (1963) Geological map of Syria 1:200 000. V.O. Technoexport, Russian Federation, Moscow

Putirka K, Johnson M, Kinzler R, Longhi R, Walker D (1996) Thermobarometry of mafic igneous rocks based on clinopyroxene-liquid equilibria, 0–30 kbar. Contrib Mineral Petrol 123:92–108

Rudnick RL, Fountain DM (1995) Nature and composition of the continental crust; a lower crustal perspective. Rev Geophys 33:267–309

Sandvol E, Seber D, Barazangi M, Vernon F, Mellors RJ, Al Amri MS (1998) Lithospheric seismic velocity discontinuities beneath the Arabian Shield. Geophys Res Lett 25:2873–2876

Schilling JG, Kingsley RH, Hanan BB, McCully BL (1992) Nd-Sr-Pb isotopic variations along the Gulf of Aden; evidence for Afar mantle plume-continental lithosphere interaction. J Geophys Res 97:10,927–10,966

Searle MP (1994) Structure of the intraplate eastern Palmyride fold belt, Syria. Geol Soc Am Bull 106:1332–1350

Sharkov YV, Chernyshev IV, Devyatkin YV, Dodonov AY, Ivanenko VV, Karpenko MI, Leonov YG, Novikov VM, Khanna S, Khatib K (1994) Geokhronologiya pozdnekaynozoyskikh bazal'tov Zapadnoy Sirii Translated Title: Geochronology of late Cenozoic basalts in western Syria. Petrologiya 2:385–394

Shaw JE, Baker JA, Menzies MA, Thirlwall MF, Ibrahim KM (2003) Petrogenesis of the Largest Intraplate Volcanic Field on the Arabian Plate (Jordan): a mixed lithosphere-asthenosphere source activated by lithospheric extension. J Petrol 44:1657–1679

Spera FJ, Bohrson WA (2001) Energy-constrained open-system magmatic processes; I, General model and energy-constrained assimilation and fractional crystallization (EC-AFC) formulation. J Petrol 42:999–1018

Stein M, Hofmann AW (1992) Fossil plume head beneath the Arabian lithosphere? Earth Plan Sci Lett 114:193–209

Walley CD (1998) Some outstanding issues in the geology of Lebanon and their importance in the tectonic evolution of the Levantine region. Tectonophysics 298:37–62

Weinstein Y, Navon O, Lang B (1994) Fractionation of Pleistocene alkali-basalts from the northern Golan Heights, Israel. Isr J Earth Sci 43:63–79

Wilson M, Downes H (1991) Tertiary-quaternary extension-related alkaline magmatism in Western and Central Europe. J Petrol 32:811–849

Yurtmen S, Rowbotham G, Isler F, Floyd PA (2000) Petrogenesis of basalts from southern Turkey: the Plio-Quarternary volcanism to the north of Iskenderun Gulf. In: Bozkurt E, Winchester JA, Piper JDA (eds) Tectonics and Magmatism in Turkey and the Surrounding Area, vol 173. Geological Society of London, London, United Kingdom, pp 489–512